Journal of the Korean Nuclear Society
Volume 30, Number 3, pp.181~193, June 1998

Improvement of Liquid Droplet Entrainment Model in the COBRA-TF Code

Kwi-Seok Ha, Jae-Jun Jeong, and Suk Ku Sim
Korea Atomic Energy Research Institute
150 Dukjin-dong, Yusong-gu, Taejon 305-353, Korea

(Received May 20, 1997)

Abstract

The COBRA-TF liquid droplet entrainment models have been assessed and improved through various experiments. The COBRA-TF code uses the Wurtz entrainment model in the film mist flow regime and the mechanistic model based on the critical Weber number and critical vapor velocity in the hot wall flow regimes, respectively. The Wurtz model has been replaced with the modified Sugawara model. The assessment against the experiments by Hewitt, Keeys, Yanai, and Whalley showed the modified Sugawara model better predicts the steam-water as well as the air-water experiments for the film mist flow regime. For hot wall flow regime, the COBRA-TF entrainment model was modified using two methods, one with an increased critical Weber number and the other with the Yonomoto' s critical vapor velocity model. The modified models were assessed using the FLECHT-SEASET bottom reflood tests. The results showed that the Yonomoto model best predicts the quenching time, whereas the local maximum rod temperature was not affected much.

1. Introduction

The COBRA-TF code was developed at the Pacific Northwest Laboratory to provide best-estimate thermal-hydraulic behaviors of nuclear reactor primary coolant systems to small and large break loss-of-coolant accidents(LOCAs) as well as the anticipated transients in pressurized water reactors (PWRs). The code provides a two-fluid and three-field representation of two-phase flow on rectangular Cartesian or subchannel coordinates. Three fields represent continuous vapor, continuous liquid, and entrained liquid droplets[1]. Because the droplet phase, which is characterized by a great ratio of surface area to volume, has quite different characteristics of heat, mass and momentum transfer from the continuous liquid phase, the droplet field is separately modeled in the COBRA-TF code.

During the reflood period of a large-break LOCA in PWRs, the fuel rod near the quench front is cooled by rapid boiling and axial thermal conduction. The emergency core cooling water supplied in excess of the quench front velocity forms a dispersed two-phase region above the quench front, and the liquid phase in the region then traverses core in droplet form. The droplets are either deposited at the upper plenum or

vented to steam generators through the hot legs. The core cooling is strongly influenced by the droplet behaviors. Droplets in the core cool down the fuel rods by reducing the superheated steam temperature. Top-down quenching can occur by droplets deposited in the upper plenum. Vaporization of droplets in steam generator tubes by heat transfer from the secondary side creates additional resistance, which in turn reduces the reflood velocity. This coupled system behavior is called steam binding effect. Therefore, accurate modeling of the droplet behaviors is very important for the large-break LOCA analysis.

This paper assesses the existing COBRA-TF droplet entrainment models and improves the models. Droplet entrainment can occur in the film mist and hot wall flow regimes. The COBRA-TF code uses the Wurtz model and a mechanistic model based on the critical Weber number and critical vapor velocity to predict the entrainment phenomena in the two flow regimes, respectively. For the case of film mist flow regime, COBRA-TF well predicts the entrained liquid mass flow rate in the high pressure range, however, shows large discrepancies in the low pressure range. This is due to the fact that the Wurtz model was mainly based on the experimental data conducted at the high pressure range of 3 ~ 9 MPa [2]. For the hot wall flow regime, the assessment using the FLECHT-SEASET reflood tests showed that COBRA-TF generally well predicts the local maximum rod temperatures, but tends to underpredict the quench front velocity, that is, the quenching time is predicted with a delay. Therefore, the following entrainment models have been implemented in COBRA-TF and these models are assessed using the experiments by Hewitt, Keeys, Yanai, and Whalley and the FLECHT-SEASET reflood tests :

- The modified Sugawara correlation in film mist flow regime,
- The original COBRA-TF model with We_d =12.0 in hot wall flow regime,
- The Yonomoto' s model in hot wall flow regime.

2. Physical Models for the Entrainment and Deposition

The COBRA-TF hydrodynamic model is a two-fluid, three-field representation of the two-phase flow system. For closure of the governing equations of the system, constitutive relations are incorporated. These include the state-of-the-art physical models for the interfacial mass transfer, the interfacial forces, the liquid and vapor wall drag, the wall and interfacial heat transfer, and the thermodynamic properties of water. The rate of entrainment/de-entrainment and a transport equation for vapor/droplet interfacial area concentration are also included.

The continuity equation for the droplet field in the COBRA-TF code is as follow :

$$\frac{\partial}{\partial t}(\alpha_e \rho_l) + \nabla \cdot (\alpha_e \rho_l U_e)$$

$$= -\Gamma_e''' + S_E''' - S_{DEL}''' - S_{DEG}''' - S_{DES}''' - S_{DEA}''' \quad (1)$$

The first term in the right-hand side of Eq. (1) represents the evaporation rate of the entrained liquid droplet, and the next terms describe the entrainment rate on continuous liquid, the deposition rate on continuous liquid, the deposition on grid spacers, the deposition on rod structures, the deposition at area changes, respectively. The entrainment/deposition between the droplet and continuous liquid phases can occur in cocurrent/counter-current film mist and hot wall flow regimes during the reflood phase of the large break LOCA. This study is focused on the entrainment models for the cocurrent film mist and hot wall flow regimes.

2.1. Entrainment and Deposition Models in the Film Mist Flow

In the film mist flow, continuous liquid flows as a film along the channel wall and the droplets disperse in the vapor core. Ishii and Grolmes[3] described the entrainment mechanisms in the wavy liquid film in terms of roll wave shearing-off, wave undercutting, droplet impingement, bubble burst and liquid bulge disintegration. The roll wave shearing-off generates droplets when gas velocities exceed those required for the inception of entrainment in annular flow. Liquid entrainment by wave undercutting occurs at low Reynolds numbers and high gas velocities. Droplets are generated by bursting of the liquid film formed at the top of bubble rising to liquid surface. Liquid bulge disintegration is important in the counter-current flow.

In the COBRA-TF, the Wurtz' s empirical correlation[4] is adopted for the droplet entrainment rate in cocurrent film flow :

$$S_E'''=0.41\left(\frac{k_s\tau_i}{\sigma}\right)\left(\frac{u_v\mu_l}{\sigma}\right) \tag{2}$$

The equivalent sand roughness k_s and the interfacial shear stress τ_i are given by

$$k_s=0.57\delta_{th}+6.625\times10^{3}\delta_{th}^{2}-3.56\times10^{6}\delta_{th}^{3}+1.5736\times10^{9}\delta_{th}^{4} \tag{3}$$

$$\tau_i=f_i\rho_v u_{vl}^2/2 \tag{4}$$

where $\delta_{th}=\frac{D_h\alpha_l}{4}$.

The interfacial friction factor f_i is calculated by the Wallis correlation[5] for stable film flow and the Henstock and Hanratty correlation[6] for unstable film flow.

Droplets are deposited on the continuous liquid as a result of random turbulent motions that impart transverse velocity to the droplets and bring them into contact with solid surfaces or liquid films within the flow channel. The COBRA-TF code uses the Cousin' s correlation to determine the deposition rate for the film flow :

$$S_{DE}'''=k_D C \tag{5}$$

where C is the mean droplet concentration in the vapor core as given by

$$C=\frac{\alpha_e\rho_l}{\alpha_e+\alpha_v} \tag{6}$$

and k_D is the mass transfer coefficient. This coefficient has been found to be a function of surface tension. This function is represented by

$$k_D=\max(3.0491\times10^{12}\sigma^{5.3054},12.491\sigma^{0.8968}). \tag{7}$$

It is found in the literature[7, 8] that the uncertainty of the entrainment models is generally greater than that of the deposition models. This is also true for the COBRA-TF models.

Sugawara adopted the Wurtz model in the FIDAS code [9], which uses a two-fluid and three-field model for two-phase flows, and he modified the Wurtz model to take into account the effects of pressure as follows :

$$S_E'''=0.219\left(\frac{\Delta h\tau_i}{\sigma}\right)\left(\frac{u_v\mu_l}{\sigma g}\right)\left(\frac{\rho_l}{\rho_v}\right)^{0.4} \tag{8}$$

where $\Delta h=\begin{cases}k_s & for\ \mathrm{Re}_v>10^5\\ k_s[2.136\log_{10}(\mathrm{Re}_v)-9.68] & for\ \mathrm{Re}_v\le10^5\end{cases}$ (9)

The deposition model in the FIDAS code considers the turbulent diffusivity of droplets as follows :

$$S_{DE}'''=9.0\times10^{-3}\left(\frac{C}{\rho_v}\right)^{-0.5}\mathrm{Re}^{-0.2}Sc^{-2/3}u_vC \tag{10}$$

The Schmidt number Sc in Eq. (10) is obtained by the Lewis relation, i.e. $Le = Sc/Pr \cong 1.0$, where Pr is the vapor Prandtl number.

Ezzidi et al.[2] modified the Sugawara' s entrainment correlation by adding a term of

Reynolds number ratio between liquid and vapor at the interface to consider the effects of liquid viscosity and mass flux. The resulting correlation is given by

$$S_E''' = 0.219\left(\frac{\Delta h \tau_i}{\sigma}\right)\left(\frac{u_v \mu_l}{\sigma g}\right)\left(\frac{\rho_l}{\rho_v}\right)^{0.4}\left(\frac{\mathrm{Re}_v}{\mathrm{Re}_w}\right)^{0.235} \quad (11)$$

$$\text{where } \Delta h = \begin{cases} k_s & \text{for } \mathrm{Re}_v > 10^5 \\ k_s[2.39232\log_{10}(\mathrm{Re}_v) - 9.68] & \text{for } \mathrm{Re}_v \le 10^5 \end{cases} \quad (12)$$

$$\text{and } \mathrm{Re}_w = \frac{u_w \rho_v D_h \alpha_v}{\mu_v}$$

They implemented Eq. (11) into the COBRA-TF code. The exponent of the Reynolds number ratio in Eq. (11) was obtained from the COBRA-TF assessment using the experiments by Hewitt et al. and Keeys et al[2]. Comparing Eqs. (9) and (12), it can be seen that the coefficient of logarithm was also changed. It is natural that the Sugawara model in the FIDAS code was calibrated in the COBRA-TF code, because the COBRA-TF and FIDAS codes use different interfacial friction models and other variables on which the entrainment rate is dependent.

2.2. The Entrainment Models During Reflood Phase

In the COBRA-TF code, the entrainment rate during reflood phase, i.e., in hot wall flow regime, is expressed as;

$$S_E = \left(\frac{\alpha_v u_v}{u_{v,crit}}\right)^2 w_v \quad (13)$$

The vapor flow rate w_v reflects the effect of boiling at the quench front on droplet formation. $u_{v,crit}$ is the critical vertical vapor velocity required to lift a droplet with a radius defined by the critical Weber criterion against gravity. The critical velocity is obtained from balance between drag and gravity forces acting on the droplet as follows :

$$u_{crit} = \left(\frac{4We_d}{3C_D}\right)^{1/4}\left(\frac{\sigma g \Delta\rho}{\rho_g^2}\right)^{1/4} \quad (14)$$

where the critical droplet Weber number We_d and the drag coefficient C_D are 2.0 and 0.45 in the COBRA-TF code, respectively.

As can be seen in Eqs. (13) and (14), the entrainment rate is a function of the critical droplet Weber number, which is defined by

$$We_d \equiv \frac{\rho_v u_v^2 D_d}{\sigma} \quad (15)$$

where D_d is the droplet diameter. A large free-falling droplet becomes unstable due to the Taylor instability and disintegrates into smaller droplets. Various values for the critical Weber number can be found in the literature. Hinze[10] obtained ~12 of the critical Weber number for droplets suddenly exposed into an air stream. For turbulent flow, he assumed 1.2 of the critical Weber number. Kataoka, Ishii and Mishima[11] obtained 8 to 17 for free falling droplets and 1.2 to 2.5 for disintegration of fluid particles by strong turbulent motions of a continuous phase. Yodar and Rohsenow [12] used 6.5 of a critical Weber number to determine initial droplet size in their analysis of the dispersed flow. In addition, the state-of-the art system analysis codes use different critical Weber numbers as follows : 8.0 in CATHARE2, 4.0 in TRAC-PF1, 3.0 in RELAP5/MOD3, 2.7 in TRAC-BF2, and 1.3 in FIDAS. It is clear that the uncertainty of the critical Weber number (in other words, the inception criterion for the liquid entrainment) is still large and the critical Weber number of 2.0 in COBRA-TF is relatively small.

Yonomoto[13] derived the inception criterion for the liquid entrainment in terms of jet instability :

$$(\alpha u)_{v,crit} = \left(\frac{3.57}{C_D}\right)\left(\frac{\sigma g \Delta\rho}{\rho_v^2}\right)^{1/4} N_{\mu v}^{1/6} \quad (16)$$

$$\text{where } N_{\mu v} = \frac{\mu_v}{(\rho_v \sigma \sqrt{\sigma / g\Delta\rho})^{0.5}}$$

$$C_D = \begin{cases} \frac{24}{\mathrm{Re}}(1 + 0.15\mathrm{Re}^{0.687}) & \text{for } \mathrm{Re} < 1000 \\ 0.44 & \text{for } \mathrm{Re} \ge 1000 \end{cases}$$

$$\mathrm{Re} = \frac{\rho_v j_v d}{\mu_v}$$

Table 1. Conditions of the Experiments by Hewitt et al., Keeys et al. and Yanai

Parameter	Hewitt et al.	Keeys et al.	Yanai	Whalley et al.
Channel flow area(m^2)	6.79×10^{-5}	1.25×10^{-4}	1.13×10^{-4}	7.94×10^{-4}
Channel wetted perimeter(m)	0.02921	0.03965	0.0377	0.0999
Tube inner diameter(m)	0.0093	0.0126	0.012	0.0318
Tube length(m)	3. 6576	3.6576	2.30	18.9
Pressure(MPa)	0.24~0.45	3.45	0.34	0.2~0.345
Mass flow rate(kg/s)	0. 02016	0. 824~0.87	0.24~0.03	0.124~0.252
Enthalpy(kJ/kg)	747.6 ~ 2530.3	1230.4~ 2791.8	795.9~ 2300.6	~2593.5

Equation (16) was obtained with the assumption that the maximum diameter of droplets generated by jet instability is determined by the surface tension and viscosity number, not by Weber number. Inserting Eq. (16) into Eq. (14) yields

$$S_E = \left(\alpha_v^2 u_v\right)^2 \left(\frac{3.57}{C_D}\right)^{-2} \left(\frac{\sigma g \Delta\rho}{\rho_v^2}\right)^{-1/2} N_{\mu v}^{-1/3} w_v \qquad (17)$$

3. Assessmemt of the Entrainment/ Deposition Models

The entrainment/deposition models described in section 2 were implemented into the COBRA-TF code and have been assessed.

3.1. Entrainment in Film Mist Flow Regime

The steam-water experiments by Hewitt et al.[14], Keeys et al.[15], and Yanai and the air-water experiments by Whalley et al.[16] were simulated using the two entrainment/deposition models. :

(i) The original COBRA-TF model (the Wurtz model) of Eqs. (2) through (5).

(ii) The modified Sugawara model of Eqs. (10) through (12).

The test data of Yanai and Whalley et al. were taken from Refs. of 9 and 16. Table 1 shows the geometry of these experiments. In steam-water experiments, slightly superheated steam and saturated water were introduced into the pipe inlet. Whereas, in the air-water experiments subcooled liquid and air were assumed to be introduced into the pipe inlet. Using measurements at two distances, it was possible to obtain some check on whether the flow had attained a hydrodynamic equilibrium state. Having established a fully developed film mist flow (that is, the rates of liquid entrainment and deposition are in hydrodynamic equilibrium), the flow rate of entrained liquid was estimated by subtraction of the film flow rate, which was measured at the outlet, from the known inlet water flow.

Hewitt' s experiment was conducted under low pressures (0.24, 0.34, 0.45 MPa) and low mass flow rate (maintained constant at 0.0202 kg/s). The inlet steam quality ranged from 10 to 90 %. Keeys' s experiment was performed under higher pressures of 3.45 and 6.89 MPa, mass flow rates of 0.17 and 0.34 kg/s, inlet steam quality ranged from 25 to 70 %. Yanai' s experiment was carried out under the low pressure of 0.34 MPa and mass flow rates of 0.0235 and 0.0314 kg/s. The range of steam quality is from 10 to 80 %. Whalley et al. conducted the air-water experiment in a very long vertical round tube compared to the other experiments. The test section length is 18.9 m and the inner diameter is 31.8 mm. These

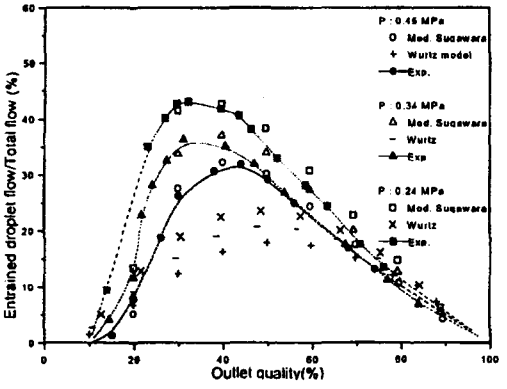

Fig. 1. Comparison of the Droplet Flow at the Outlet : Hewitt' s Experiment.

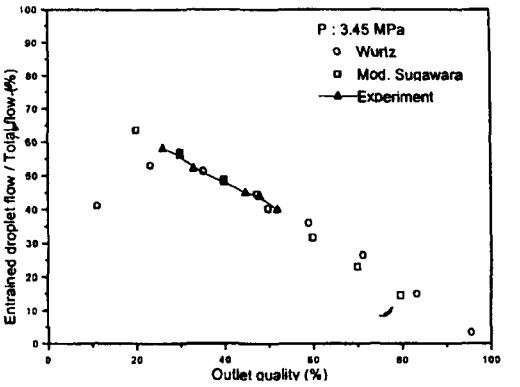

Fig. 2. Comparison of the Droplet Flow at the Outlet : Keeys' Experiment

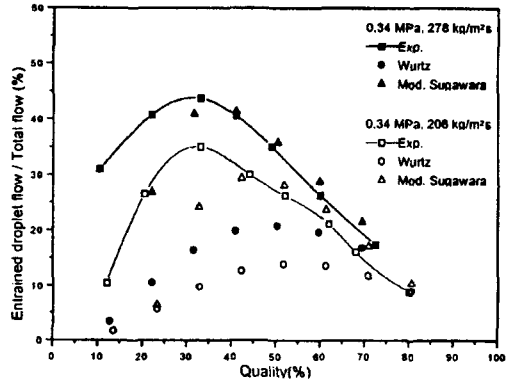

Fig. 3. Comparison of the Droplet Flow at the Outlet : Yanai' s Experiment

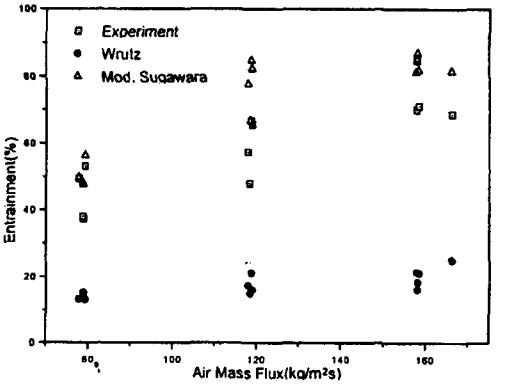

Fig. 4. Comparison of the Droplet Flow at the Outlet : Whalley' s Experiment

tests has the pressure range of 0.203 to 0.345 MPa. The mass fluxes extend over 48.1 to 166.2 kg/m^{2}s for air and 23.7 to 190.0 kg/m^{2}s for liquid.

The COBRA-TF input model for the steam-water experiments consists of a channel with equal-length cells and appropriate boundary conditions. The number of cells was 48 for the experiments by Hewitt and Keeys and 30 for the experiment by Yanai. Total mass flow rate is given at the inlet and a constant pressure is set at the outlet. The input model for the air-water experiments consists of two sections with three channels. Section 1 is composed of two channels to inject air and liquid respectively. Section 2 models the test section, which consists of single channel with 25 cells.

Figure 1 compares the percent of the predicted droplet flow rate at the exit with the Hewitt' s (low-pressure) experimental data. As mentioned previously, the original COBRA-TF model greatly underpredicts the droplet flows, especially in mid-quality conditions, because the Wurtz model was developed using high pressure experimental data. However, the results of the modified Sugawara model show an excellent agreement with the data in the whole quality range. The predictions of Keeys (high-pressure) experiments are shown in Fig. 2. Both the original Wurtz and the modified

Table 2. Predictions of Experimental Data for Air-Water Flow

	Experimental Conditions			Entrained liquid fraction(WE/ WE +WF)		
Exp. No.	Air Mass Flux(kg/m^{2}s)	Liquid Mass Flux(kg/m^{2}s)	Pressure (MPa)	Experiment	Wurtz	Mod. Sugawara
201W	58.0	1160.3	0.270	0.847	0.160	0.851
202W	77.8	160.3	0.279	0.493	0.129	0.497
205W	157.8	78.1	0.279	0.700	0.214	0.813
206W	78.9	79.3	0.279	0.373	0.150	0.476
207W	158.1	160.3	0.269	0.855	0.183	0.869
208W	79.3	160.3	0.269	0.530	0.128	0.562
209W	158.4	79.9	0.276	0.711	0.211	0.818
210W	78.7	79.9	0.276	0.380	0.149	0.481
603W	166.2	71.0	0.270	0.687	0.250	0.815
605W	118.9	118.6	0.269	0.655	0.158	0.822
1104W	117.9	79.9	0.270	0.573	0.171	0.777
1204W	118.4	79.9	0.345	0.479	0.147	0.667
1304W	118.7	79.9	0.203	0.667	0.211	0.847

Sugawara models predict the droplet flow rates well.

But, it should be noted that the Sugawara model was calibrated against the experiments by Hewitt and Keeys. Thus, the other experiments by Yanai and Whalley et al. were simulated to further assess the modified Sugawara model. Yanai conducted basically similar experiment with Hewitt and Keeys, but used a different mixing device. Figure 3 compares the calculated and measured droplet flow rates. The original COBRA-TF greatly underpredicts the droplet flow rates. The modified Sugawara model reasonably predicts the droplet flow rates but the discrepancy increases as the quality decreases. This discrepancy is caused by different initial entrainment fraction at the entrance of test section[9]. In these experiments, droplets initially exist by using the mixing device. Unfortunately the COBRA-TF code could not consider this effect as a boundary condition.

Figure 4 shows the comparison of the results of each model against the experiment by Whalley et al. As shown in Table 2, a wide range of liquid and air flow rates have been chosen for the comparison of the two models. Here entrained liquid fraction is defined as entrained liquid flow(W^E)/total liquid flow(W^E+W^F). Because of the strong dependency on air flow rate, the entrained flow rates were compared as functions of the air flow rate in Fig. 4. The Wurtz model underestimates the entrained liquid flow rate in whole range of air flow rates, however, the modified Sugawara model predicts the data with a good accuracy. It is apparent, from Figs. 1 through 4, that the modified Sugawara model better predicts the experimental data than the Wurtz model.

3.2. Entrainment in Hot Wall Flow Regime

According to the results of the International 2D/3D program, 10 to 40 % of the core inlet flow during the bottom reflood was carried over, that is, entrained in steam flow. Therefore, the entrainment phenomenon strongly affects the reflood heat transfer and quench front advancement[17]. In order to assess the entrainment model of the COBRA-TF code in hot wall flow regime, FLECHT-SEASET tests were

Table 3. The Initial Conditions of Selected Tests

Test No.	Peak power (kW/m)	Flooding rate (mm/s)	Pressure (MPa)	Initial temp.(K)	No. of dis-connected rods
31805	2.3	21.6	0.2758	1144	2
32013	2.3	26.4	0.4137	1160	2
30817	2.3	38.6	0.2689	804	2
34006	1.3	15.0	0.2689	1155	10
34610	1.4	21.0	0.1379	1165	10
34524	3.0	39.9	0.2758	1151	10

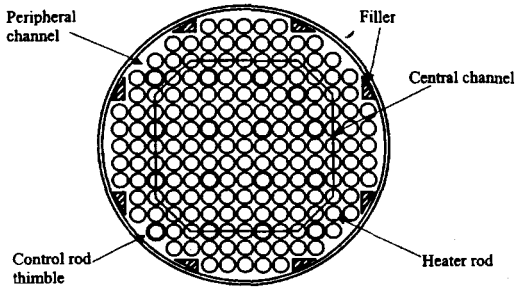

Fig. 5. Radial Nodding for FLECHT-SEASET 161-Rod Bundle Tests.

used in this study. The FLECHT-SEASET tests were conducted to understand the two-phase flow phenomena and to develop the computer code to analyze the thermal hydraulics in the rod bundle during reflood phase of a large break LOCA. The details of the tests are described in the NUREG/CR-1532 report[18].

Using the FLECHT-SEASET 161 rod bundle forced reflood tests, three entrainment models in hot wall flow regime have been assessed :

(i) The original COBRA-TF model of Eqs. (13) through (15).

(ii) The original COBRA-TF model with We_d =12.0.

(iii) The Yonomoto' s model of Eq. (17).

Six forced reflood tests among the FLECHT-SEASET tests are selected to evaluate the liquid entrainment models during bottom reflood. Table 3 summarizes the experimental conditions for the

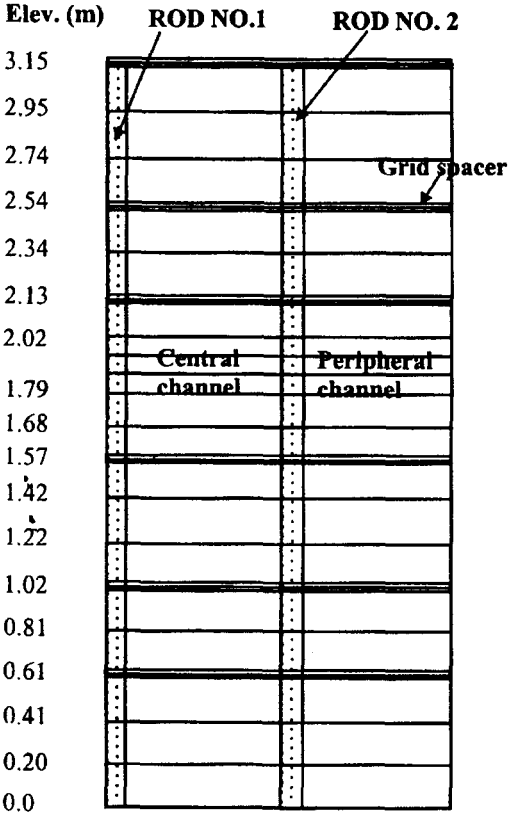

Fig. 6. Axial Nodalization for FLECHT-SEASET Tests

selected tests. In case of the low power and low flooding rate, it is more likely to form a film mist flow. Whereas, an inverted annular flow (hot wall flow regime) is formed in the high power and high flooding rate. Therefore, tests with various

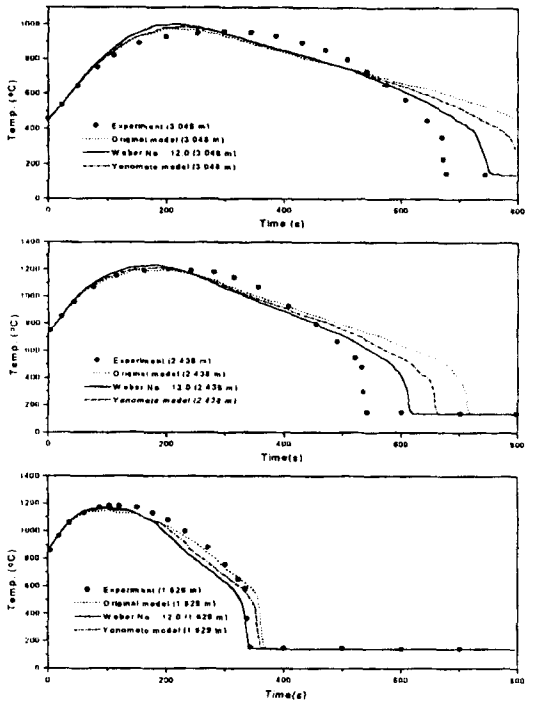

Fig. 7. Heater Rod Temperature Behaviors of FLECHT-SEASET Test 31805.

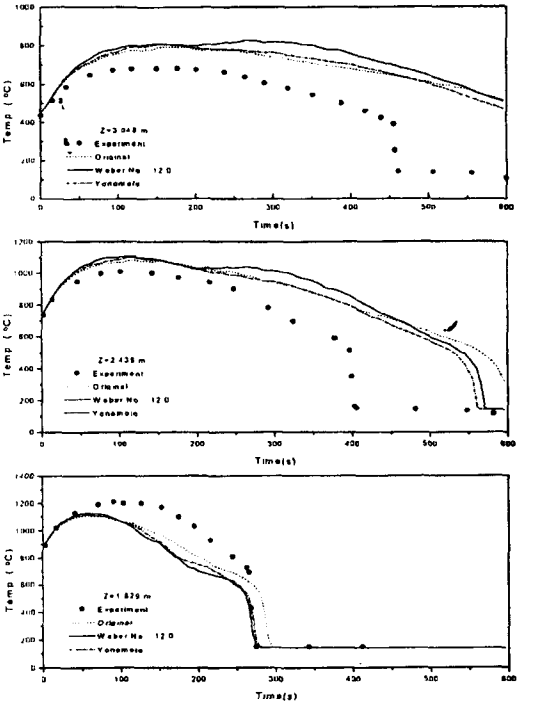

Fig. 8. Heater Rod Temperature Behaviors of FLECHT-SEASET Test 34524

conditions are chosen so that the models can be fully assessed for two types of the film-mist flow and inverted annular flow in the hot wall flow regime near the quench front.

Figures 5 and 6 show the schematic of the test section and the COBRA-TF nodalization. The test section consists of 161 heater rods arranged in square pitch with dimensions comparable to 17 × 17 PWR fuel rods. The diameter of the heater rod is 9.5 mm and the rod pitch is 12.6 mm. The bundle also contains sixteen control rod guide tubes of 12.0 mm diameter and eight solid fillers. The test section length is 3.6576 m. The bundle flow area is 0.01568 m^2 and grid spacers are located at 0.5207 m intervals. The radial power profile is flat and the axial power profile is a chopped cosine shape with the peak to average ratio of 1.66.

The COBRA-TF input model consists of two channels : one for the central region and the other for the peripheral region as shown in Fig. 5. Each channel has 19 cells. Rods 1 and 2 in Fig. 6 represent the heater rods within channels 1 and 2, respectively. Initial temperatures of the heater rods and unheated conductor (housing and guide tube) are specified using the measured values at the beginning of the reflood test. Inlet mass flow rates and exit pressures are given as boundary conditions.

Figures 7 and 8 compares the rod surface temperature behaviors of Test 31805 and 34524 at three different elevations. In general, the three models predicts almost the same local maximum rod temperatures, but different quenching times. As shown in Figs. 7 and 8, the local maximum rod temperatures are well predicted in the lower and mid elevations, however, in the upper part, the temperatures are somewhat high and the

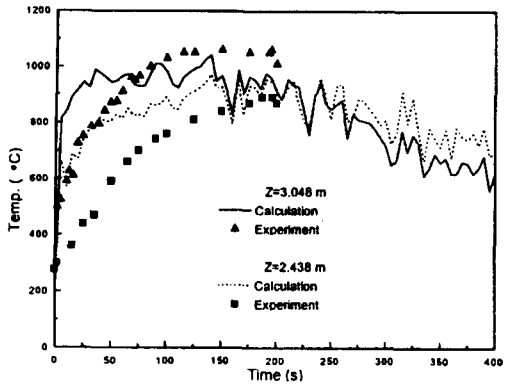

Fig. 9. Steam Temperature Behaviors of FLECHT-SEASET Test 31805.

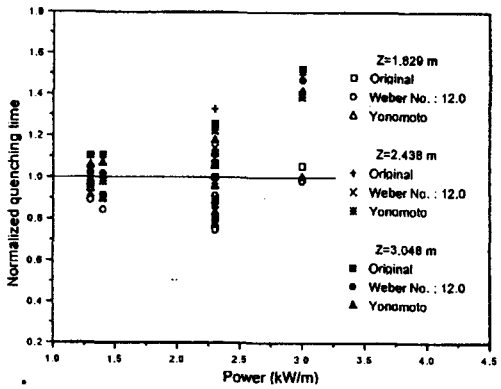

Fig. 10. Quenching Time vs. Power : FLECHT-SEASET

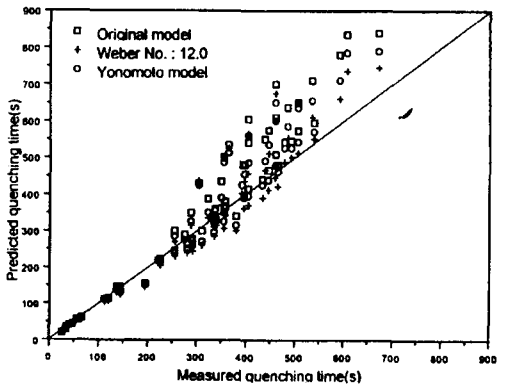

Fig. 11. Comparison of the Quenching Times : FLECHT-SEASET.

quenching times are delayed. In Eq. (13), the liquid entrainment rate is directly proportional to the steam flow. With the advance of the quench front, more steam is generated. As a result, more droplets are formed and, in turn, the quenching time is more delayed. Generally, the three models seem to overpredict the entrainment. Thus, after ~250 s in Fig. 7, the predicted heater rod temperatures are lower than the measured values. The calculation results of all the tests except Test 34524 showed similar trends.

Test 34524 was carried out under high power and high flooding rate. In this test, top-down quenching occurred. But, as shown in Fig. 8, the code failed to predict this phenomenon because the upper volume of the test section was not properly modeled. In addition, the calculation results showed great rewet effect of the grids because the deposition rate on the grid is directly proportional to the steam flow. And thus, this test represents the large entrainment rate and the great deposition rate. For this reason, heater rod temperatures at 1.829 m (just below the grid) are lower than test data, while temperatures at 2.438 and 3.048 m (just above the grid) are higher than data. This phenomenon is due to the increase of heat transfer between the steam and the droplet.

Comparison of the measured and calculated steam temperatures for Test 31805 is given in Fig. 9. Until~60 s, the calculated steam temperature at 3.408 m is higher than the measured. This is due to the delayed inception of liquid entrainment. The inception of liquid entrainment was started at 10 seconds[19] in experiment, on the other hand, it was started at 30 s, 40 s, and 35 s with the original COBRA-TF model, the original COBRA-TF model with We_d=12, and the Yonomoto model, respectively. Since the droplets cool down the superheated steam, the delayed inception of liquid entrainment

results in greater superheating of the steam. After 60 s, droplet entrainment occurs sufficiently and, then, the calculated steam temperature tends to decrease below the experimental data. This seems to be related with excessive liquid entrainment.

In general, the model with We_d=12 predicts higher heater rod temperatures because of later inception of entrainment and smaller droplet flow in comparison with the original model of COBRA-TF. However, the prediction of quench front is faster than other models due to reduced entrainment rate (see Eqs. (13) and (14)). On the other hand, the Yonomoto model predicts temperatures and quenching times between those of the original model and the model with We_d=12.

Figures 10 and 11 show the quenching times at 1.829, 2.438 and 3.048 m. It can be seen that the difference between the calculations and the experiments increases as either the elevation or power increases. Generally, the model with We_d=12 predicts the quenching time earlier than other models, and the original model predicts the most delayed quenching.

To systematically analyze the results, the calculated quenching times for the three models are fitted as a linear function of the measured data using a least-square approach. For convenience, let' s define a dimensionless quenching time as

$$\phi(t) = \frac{t(z) - t_{min}(z)}{t_{min}(z)} \tag{18}$$

where $t(z)$ = quenching time at elevation z.

u_{in} = the injected water velocity.

$t_{min}(z)$ is the quenching time at elevation z when we assume that the water injected into the bottom of the test section moves upward like a piston, that is, without phase change and entrainment, and that the quenching occurs at the water column front. Both the experiment and the calculation results showed that $t(z)$ is always greater than $t_{min}(z)$. This is mainly due to the steam generation and the liquid entrainment near the quench front. The difference in quenching times has a great influence on the entrainment. Therefore, can be used as a dimensionless measure for evaluating the entrainment models.

The linear function for the least-square analysis is as follows ;

$$P_i = aM_i + b \tag{19}$$

where P_i and M_i stand for the predicted and the measured dimensionless quenching time, respectively. The coefficients of the a and b are obtained from minimizing following equation :

$$f(a,b) = \sum_{i=1}^{N}(aM_i + b - P_i)^2 \tag{20}$$

where N is the number of data. Because, in the high elevations, the calculated values show large errors, 42 data are taken in the upper part and 18 data in the lower part of the test section. After obtaining a and b, the deviation from the fitting line (DFL) and the deviation from the experimental data (DED) are calculated as follows :

- Deviation from Fitting Line (DFL);

$$E_F = \frac{1}{N}\left[\sum_{i=1}^{N}(aM_i + b - P_i)^2\right]^{1/2} \tag{21}$$

- Deviation from Experimental Data (DED);

$$E_P = \frac{1}{N}\left[\sum_{i=1}^{N}(M_i - P_i)^2\right]^{1/2} \tag{22}$$

The results of the least-square analysis are listed in Table 4. The model with We_d=12 reduces the DED but increase the DFL (i.e., the scatter increases), while the Yonomoto model reduces both the DED and the DFL in comparison with the original model. Therefore, in terms of

Table 4. Least-Square Analysis of the Dimensionless Quenching Time

Model	a	b	DFL(E_f)	DED(E_p)
Original model	1.463	−0.736	0.089	0.143
We_d=12	1.416	−0.954	0.094	0.125
Yonomoto	1.384	−0.734	0.084	0.119

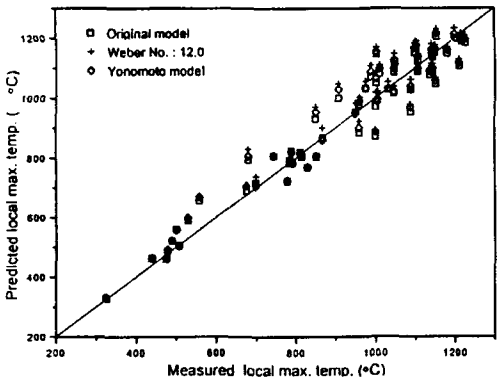

Fig. 12. Comparison of the Local Maximum Rod Temperatures : FLECHT-SEASET.

quenching time, the Yonomoto model is the best among the three models. Figure 12 compares the local maximum rod temperatures, which shows each model predicts the rod temperatures reasonably well compared to the quenching times.

4. Conclusions

To improve the liquid entrainment model of the COBRA-TF, the following entrainment models have been implemented in the code and these models are assessed using the experiments by Hewitt, Keeys, Yanai, and Whalley and the FLECHT-SEASET reflood tests :

- The modified Sugawara correlation in film mist flow regime,
- The original COBRA-TF model with We_d =12.0 in hot wall flow regime,
- The Yonomoto' s model in hot wall flow regime.

For the entrainment in the film mist flow regime, the modified Sugawara model shows good agreements for the steam-water experiments as well as air-water experiments. For the entrainment in the hot wall flow regime, the COBRA-TF model with We_d =12.0 and Yonomoto model were assessed against the FLECHT-SEASET forced reflood test data. Yonomoto model best predicts the quenching time, whereas the predicted local maximum rod temperatures were not significantly different between the models.

Therefore, the Sugawara and the Yonomoto models are recommended for the liquid droplet entrainment models in film mist flow and hot wall flow regimes, respectively. For further improvement on the quench time prediction of the COBRA-TF code, other models such as the deposition on grid spacers and the gap conductance have to be assessed.

References

1. M. J. Thurgood, J. M. Kelly, T. E. Guidotti, R. J. Kohrt and K. R. Crowell, "COBRA/TRAC - A Thermal-Hydraulics Code for Transient Analysis of Nuclear Reactor Vessels and Primary Coolant Systems", NUREG/CR-3064, Vol. 1 ~ 5 (1983).
2. A. Ezzidi, T. Okubo, and Y. Murao, "Improvement of COBRA-TF code models for liquid entrainments in film-mist flow", JAERI-M 93-133, (1993).
3. M. Ishii, and M. A. Grolmes, "Inception Criteria for Droplet Entrainment in Two-Phase Concurrent Film Flow", AIChE Journal Vol. 21, No. 2 (1975).
4. J. Wurtz, "An Experimental and Theoretical Investigation of Annular Steam-Water Flow in Tubes and Annuli at 30 to 90 bar", RISO Report No. 372 (1978).
5. G. B. Wallis, "One-Dimensional Two-Phase Flow", McGraw-Hill, New York (1969).

6. W. H. Henstock and T. J. Hanratty, "The Interfacial Drag and the Height of the Wall Layer in Annular Flows", J. of AIChE, Vol. 22 (1976).
7. J. J. Jeong, K. S. Ha and W. P. Chang, "A State-of-the-art Report on Modeling of Liquid Entrainment Phenomena in Two-Phase Flow", KAERI/AR-450/96 (1996).
8. V. Stevanovic and M. Studovic, "A Simple Model for Vertical Annular and Horizontal Stratified Two-phase flows with liquid entrainment and Phase Transitions : One-dimensional Steady State Conditions", Nuclear Engineering and Design, Vol. 154 (1995).
9. S. Sugawara, "Droplet deposition and entrainment modeling based on the three-fluid model", Nuclear Engineering and Design, Vol. 122 (1990).
10. J. O. Hinze, "Fundamentals of the Hydrodynamic Mechanism of Splitting in Dispersion Processes", AIChE. Journal, Vol. 1, No. 3(1955).
11. I. Kataoka, M. Ishii and K. Mishima, "Generation and Size Distribution of Droplet in Annular Two-Phase Flow", J. of Fluids Engineering, Vol. 105 (1983).
12. G. L. Yoder and W. M. Rohsenow, "A Solution for Dispersed Flow Heat Transfer Using Equilibrium Fluid Conditions", J. of Heat Transfer, Vol. 105 (1983).
13. T. Yonomoto, "A Study of Entrainment at a break and in the core during SBLOCA in PWR", JAERI-R 96-024 (1996).
14. G. F. Hewitt, et al., "Liquid Entrainment in Adiabatic Steam-Water Flow", AERE-R 5374 (1969).
15. R. K. F. Keeys, et al., " Liquid Entrainment in Adiabatic Steam-Water Flow at 500 and 1000 psia", AERE-R 6293 (1970).
16. T. Saito et al, "Multi-fluid modeling of annular two-phase flow", Nuclear Engineering and Design, Vol. 50 (1978).
17. P. S. Damerell et al.(edited), "Reactor Safety Issues Resolved by the 2D/3D program", NUREG/IA-0127, GRS-101, MPR-1346, p. 2-6, USNRC (1993).
18. M. J. Loftus et al, "PWR FLECHT-SEASET Unblocked Bundle, Forced and Gravity Reflood Task Volume 1", EPRI NP-1459 (1981).
19. C. Y. Paik et al, "Analysis of FLECHT-SEASET 163-Rod Blocked Bundle Data Using COBRA-TF", EPRI NP-4111 (1986).